



Pediatric Brain White Matter Lesions: Patterns of Disorders in Suez Canal Area as Seen by Magnetic Resonance Imaging

Radwa Abd El Gawad Khalil¹, Tarek Hassan Khalil², Azza Abdelhamid Gad², Marwa A. Ibrahim³, Walid Mosallam⁴

1 Assistant lecturer of Radiology, Faculty of medicine, Suez Canal University

2 Professor of Radiology, Faculty of medicine, Suez Canal University

3 Lecturer of Pediatrics, Faculty of medicine, Suez Canal University

4 Associate professor of Radiology, Faculty of medicine, Suez Canal University

Abstract

Background: White matter diseases, also known as leukoencephalopathies, encompass a broad spectrum of disorders prevalent in the pediatric population. Magnetic Resonance Imaging (MRI) is the modality of choice for assessing patients with white matter signal abnormalities; however, diagnosing pediatric white matter disorders poses significant challenges for radiologists. The study aims to assess the role of MRI in defining different patterns of white matter lesions in the pediatric age group. **Methods:** This cross-sectional observational study was held in the MRI unit at the Radiology Department at Suez Canal University Hospital. The study included 72 eligible infants and children, with MRI evidence of white matter abnormality. **Results:** Seventy-two infants and children, 35 (48.6%) males and 37 (51.4%) females, showing MRI white matter signal abnormalities, were included in our study. Cases were classified based on MRI white matter signal changes in T1WI and T2WI into two main categories: hypomyelination (21%) and dys/demyelination pattern (74%) with 4 cases (5%) displayed as other different patterns. The sensitivity and specificity of MRI to accurately detect hypomyelination patterns in patients with hypomyelination disorders were 92.3% and 94.9% respectively, yielding an overall accuracy of 94.4%. For dys/demyelination patterns in patients with known dysmyelinating or demyelinating disorders, sensitivity was 88.1% and specificity was 92.3%, resulting in an accuracy of 88.9%. Notably, the classification of dys/demyelination patterns into confluent and multifocal types showed statistical significance; two-thirds of cases with a confluent pattern were ultimately diagnosed as dysmyelinating disorders, whereas two-thirds of those with a multifocal pattern were diagnosed as demyelinating disorders. **Conclusion:** A thorough assessment of various MRI sequences to determine the pattern and distribution of white matter abnormalities, along with evaluation for associated findings such as basal ganglia, brainstem or cerebellar abnormalities, and cortical malformations, is essential. This comprehensive approach aids in narrowing down the differential diagnosis, establishing a definitive diagnosis, or directing further investigations necessary for accurate diagnosis.

517

KeyWords: white matter; hypomyelination; dys/demyelination; MRI.

DOI Number: 10.48047/nq.2024.22.5.nq25052

NeuroQuantology 2024; 22(5):517-527

Introduction:

The human brain is composed of two distinct types of tissue: gray matter, which houses neuronal cell bodies, and white matter, which consists of nerve fibers and myelin. Myelin is essential for normal motor, sensory, and cognitive functions when myelin is absent or damaged, the brain functions become hampered

or lost (1). The process of myelination is a continuous sequential process with an orderly and predictable course. It begins within the caudal brain stem and advances rostrally to the forebrain, with the most rapid and dramatic period of human central myelination within the first two years of postnatal life (2). Evaluation of the myelination can be easily done by Magnetic resonance imaging



(MRI), as myelin deposition is associated with a shortening of the T1-weighted (T1WI) images and T2-weighted (T2WI) images, so signals of white-matter myelinated structures change from low to high on T1WI images

and from high to low on T2WI images, both relative to grey-matter signal intensity which remains more or less unchanged (3). Studying the progression and degree of myelination in the brain by MRI is the first step in pediatric neuroimaging (4).

Leukoencephalopathies, also known as white matter diseases, encompass a range of disorders that predominantly or exclusively affect the brain's white matter. These conditions are characterized by various underlying pathologies and can be classified based on the specific myelin pathology involved: dysmyelination, demyelination, hypomyelination, and delayed myelination (5). Dysmyelinating diseases, commonly referred to as leukodystrophies, arise from inherited enzyme deficiencies that lead to abnormal formation, degradation, or turnover of myelin. In contrast, demyelinating diseases involve the destruction of otherwise normal myelin. These can be classified as primary conditions, such as acute disseminated encephalomyelitis (ADEM) and multiple sclerosis, or secondary to factors like toxins, hypoxic-ischemic injury, and viral infections (6). Hypomyelination denotes a persistent deficiency of myelin due to structural and functional abnormalities in myelin sheaths, resulting in inadequate myelin production (5). MRI is the preferred modality for assessing patients with white matter signal abnormalities. However, the interpretation of white matter disorders poses significant challenges for radiologists. While MRI demonstrates high sensitivity in identifying leukoencephalopathies, recent studies indicate that its specificity is comparatively low. This lack of specificity is particularly evident as leukoencephalopathies with diverse pathophysiological origins can exhibit similar signal intensity changes on T1WI and T2WI images (2).

The study aims to assess the role of multiparametric MRI in defining different patterns of white matter lesions in the pediatric age group and establishing appropriate diagnoses.

Methods

Ethical Statement

The current study followed the STARD reporting guidelines [17]. Our institutional review board approved this study (Approval number: 4158), and each patient provided informed written consent. We adhered to the ethical precepts of the Helsinki Declaration.

Study design and population

We held this unicentric prospective study on 72 eligible infants and children with clinically suspected white matter disease enrolled from the pediatric department to the radiology department for MRI between January 2022 and December 2023. Inclusion criteria were: (I) Pediatric age group (from age of 1 day to 18 years suspected to have white matter diseases irrespective of their maturity state), and (II) MRI evidence of white matter abnormality is seen as an abnormal signal. The following patients were excluded: (I) Patients with perinatal hypoxic-ischemic encephalopathy, (II) Those with imaging findings suggesting neoplastic disease, (III) History of recent trauma, and (IV) Patients with relative or absolute contraindication to MRI examination (e.g. dental implant). All subjects of the study were assessed by detailed history (age, gender, consanguinity, and presenting symptoms), clinical examination, laboratory, and MRI examination.

MRI protocol

MRI brain was done on a 1.5 Tesla MR scanner (Philips Medical Systems, Achieva 1.5T A-series) and included: axial T1WI, T2WI & FLAIR sequences, Coronal and sagittal FLAIR sequences, diffusion-weighted (DWI) images were obtained in three orthogonal planes with b-value 0, 500, 1000 s/mm² and ADC maps. For patients aged less than 2 years the sequences parameters were: T1WI weighted spin echo (TR=500 ms, TE=15 ms), T2WI weighted fast spin echo (TR=4000 ms, TE=90-160 ms), FLAIR (TR=3500 ms, TE=30 ms, TI= 1000 ms) and DWI images (TE=6000 ms, TI= 90 ms). Adjust the field of view (FOV) and slices to best fit the patient's age and size: 0-2 years: 3mm slices / 1mm gap / small FOV and 2-5 years: 4mm slices / 1mm gap / small FOV.

MRI images analysis

Each case was analyzed based on conventional sequences including T1WI, T2WI, FLAIR, DWI, and ADC images as illustrated in the flow chart (Figure 1):

Based on conventional images including T1WI & T2WI:

Images were categorized based on the signal



intensity of white matter observed on T1WI and T2WI sequences, leading to the identification of two primary groups:

Hypomyelination Group: This group is

characterized by mild hyperintense signals on T2WI images, while T1WI images exhibit mild signal intensity, which may be hypo-, iso, or mildly hyperintense. Patients within this group were monitored after a six-month interval, following their first year of life.

Dys/demyelination Group: In contrast, this group presents with more pronounced alterations in white matter signal intensity, specifically showing hyperintense signals on T2WI and hypointense signals on T1WI images.

The classification of signal intensity into mild or non-mild categories relies primarily on subjective visual assessment. The images, the grades of the signal intensity, and hence plotting them in their specific category were done by three expert observers 10-year experience in neuroradiology blind to the clinical data, each radiologist independently interprets the images. In cases of disagreement between the three radiologists, images were re-reviewed together and a consensus (grading of signal intensity) was achieved.

Dys/demyelination group was further divided according to the extent of white matter involvement into Confluent and Multifocal patterns.

A-Confluent pattern:

Was subdivided into bilaterally symmetrical and asymmetrical

1-Confluent bilateral symmetrical pattern:

This group was classified into:

a-Diffuse pattern: Periventricular and subcortical white matter are diffusely involved.

b-Periventricular pattern: involves the periventricular supratentorial white matter only with sparing of the subcortical white matter.

c-Subcortical pattern: involves the subcortical white matter only sparing the periventricular white matter.

d-Lobar predominance: confluent bilateral involvement of the white matter of certain lobe: frontal, parietal, occipital or temporal.

2- Confluent asymmetrical pattern:

This pattern was classified based on site of the white matter predominance into:

a-Confluent asymmetrical periventricular

B-Confluent asymmetrical subcortical patterns.

B- Multifocal pattern:

Was divided into:

Patchy hyperintensities (size > 5 mm, which could be periventricular, subcortical or periventricular & subcortical).

White matter foci: size < 5 mm.

Based on DWI & ADC:

All cases were evaluated for the presence of diffusion restriction (seen as high signal in DWI in B value 1000 and low in ADC in any of the affected areas. Cerebellar atrophy, cortical malformations, cerebellar hyperintensities, diffusion restriction, basal ganglia (BG) changes and brain stem were investigated to determine their relationship with the significantly correlated MRI white matter pattern observed in the MRI scans.

In each case, the primary diagnosis was established based on clinical data and MRI findings. Subsequently, the final diagnosis was determined through a combination of reference tests, including genetic whole exome sequencing, specific laboratory tests, close follow-up, and clinical response evaluations. Finally, the primary diagnoses were compared to the final diagnoses, excluding cases classified in the nonspecific group, to calculate the prevalence of accurate diagnoses derived from combined clinical assessments and MRI findings. Based on the final diagnosis, the cases were categorized into two groups: hypomyelination and dys/demyelination. These classifications were correlated with the hypomyelination and dys/demyelination patterns identified through MRI, allowing for an evaluation of MRI accuracy in detecting these patterns. We assessed the inter-reader agreement among three observers in the evaluation of MRI images, specifically categorizing the cases into patterns of hypomyelination and dys/demyelination.

Statistical analysis

We used IBM Statistical Package for Social Sciences software (SPSS), 21st edition, IBM, United States for data analysis. Comparison between groups was done by the Chi-Square test. Wilcoxon signed ranks test was used for comparison within the group. We tested Quantitative data for normality by the Kolmogorov-Smirnov test. Normally distributed data was presented as mean + SD (Standard Deviation). We used the student t-test to compare between two



groups. Statistical significance was $P < 0.05$. The inter-reader agreement was estimated using the Fleiss-kappa test. Kappa values of less than ≤ 0 , 0.01–0.20, 0.21–0.40, 0.41– 0.60, 0.61–0.80, and more than 0.81 indicate no, slight, fair, moderate, substantial, and perfect agreement, respectively.

Results

A total of seventy-two infants and children were included in our study, comprising 48.6% males (n=35) and 51.4% females (n=37), all of whom exhibited MRI evidence of white matter signal abnormalities. The mean age of the participants was 61.08 months, with a range from 12 to 107.7 months. Additionally, 33.3% (n=24) of the subjects had a history of positive consanguinity between their parents. The main presenting symptom was neurodevelopmental delay 45.8 % (n=33) while hypotonia was the main presenting sign 26.4% (n=26).

MRI patterns of white matter disorders (Table 1):

The MRI findings regarding white matter abnormalities indicate that the predominant pattern observed was dys/demyelination, present in 73.6% (n=53) of the patients. The hypomyelination pattern was noted in 20.8% (n=15), while only 5.6% (n=4) exhibited other distinct patterns. Among the dys/demyelination group, the majority of confluent patterns were bilateral and symmetrical (n=14), as opposed to asymmetrical (n=6). In contrast, the multifocal pattern included both patchy (n=19) and closely grouped foci (n=14).

Table 1: Patterns abnormal white matter signal by MRI

Patterns of White matter signal abnormalities on MRI (N= 72)	
Hypomyelination pattern	15 (20.8 %)
Dys/demyelination pattern	53 (73.6 %)
• Confluent pattern	20 (28)
• Bilaterally symmetrical	14 (19.4)
Diffuse	7 (9.7)
Periventricular	2 (2.7)
Subcortical	0
Lobar predominance	5 (6.9)
• Asymmetrical	6 (8.3)
Periventricular	5 (6.9)
Subcortical	1 (1.4)
• Multifocal pattern	33 (46)
• Patchy	19 (26.4)
Periventricular	5 (6.9)
Subcortical	9 (12.5)
Periventricular & subcortical	5 (6.9)
• Foci	14 (19.4)
Other patterns	4 (5)

Final diagnosis groups (Table 2):

The final diagnoses were categorized into six

primary groups of disorders: hypomyelination (18.1%, n=13), inborn errors of metabolism (IEM) (16.7%, n=12), congenital muscular dystrophy (CMD) (9.7%, n=7), acquired demyelinating syndromes (ADs)(20.8%, n=15), secondary demyelination (18%, n=25), and non-specific disorders (9.7%, n=7). Pelizeus-Merzbacher disease (PMD) is the most prevalent disorder within the hypomyelination group, accounting for 11.1% (n=8/11) of cases. In contrast, Leigh syndrome represents the most frequently diagnosed condition among IEM, comprising 4.2% (n=3), followed closely by maple syrup urine disease and homocystinuria, each with 2 cases (2.8%)

Merosin-deficient CMD was the most prevalent condition among the CMD, accounting for 5.6% (n=4/7). In the category of ADs, ADEM represented more than half of the cases (n=8/15; 11.1%), while multiple sclerosis accounted for 5.6% (n=4). Among secondary demyelination causes, congenital cytomegalovirus infection was the most common, observed in 4 out of 18 cases, followed by acute necrotizing encephalopathy of childhood (ANEC) and herpes simplex virus encephalitis, each with 2 cases. Additionally, seven cases (9.7%) exhibited non-specific MRI findings of these, only one case (1.4%) demonstrated bilateral mesial hippocampal sclerosis.

Table 2: Classification of final diagnoses of the studied cases into 6 main groups of disorders.



Final diagnosis groups of disorders	No.
Hypo myelination	13 (18.1)
PMD	8 (11.1)
Hypomyelination with Down	2 (2.8)
Hypomyelination with ADDEE	1 (1.4)
GMI Gangliogliosis	1 (1.4)
Severe phenotype of POLR3A variant with strial involvement, Hypomyelination 7	1 (1.4)
Inborn errors of metabolism (IEMs)	12 (16.7)
Leigh syndrome	3 (4.2)
Maple Syrup urine disease	2 (2.8)
Homocystinuria	2 (2.8)
Adreno-leukodystrophy	1 (1.4)
Metachromatic Leukodystrophy	1 (1.4)
Isovaleric academia	1 (1.4)
Propionic academia	1 (1.4)
Gluteric aciduria type 1 (GA1)	1 (1.4)
Congenital muscular dystrophies (CMD)	7 (9.7)
Merosin-deficient congenital muscular dystrophy (MDC 1A)	4 (5.6)
Congenital muscular dystrophy 1C (MDC 1C)	1 (1.4)
Muscle-eye-brain disease (MEB)	1 (1.4)
Walker -Warburg syndrome (WWS)	1 (1.4)
Acquired demyelinating syndromes (ADS)	15 (20.8)
Acute disseminated encephalomyelitis (ADEM)	8 (11.1)
Multiple sclerosis (MS)	4 (5.6)
MOGAD antibody-associated disorders (MOGAD)	1 (1.4)
AQP4 +ve Neuromyelitis optica spectrum disorders (NMOSD)	2 (2.8)
Secondary demyelination	18 (25)
Acute necrotizing encephalopathy of childhood (ANEC)	2 (2.8)
Herpes (HSV) encephalitis	2 (2.8)
Corpus callosum impingement syndrome (CCIS) and white matter injury secondary to prolonged hydrocephalus	1 (1.4)
Carbon monoxide (CO) poisoning	1 (1.4)
PRES (posterior reversible encephalopathy syndrome)	1 (1.4)
Congenital CMV (Cytomegalovirus) infection	4 (5.6)
Congenital infection (Toxoplasmosis)	1 (1.4)
Extrapontine myelinolysis (central osmotic demyelination)	1 (1.4)
Lissencephaly with pontocerebellar hypoplasia	1 (1.4)
Post vaccination viral encephalitis	1 (1.4)
Postictal changes	1 (1.4)
Tuberous sclerosis	2 (2.8)
Nonspecific	7 (9.7)
Non specific	6 (8.3)
Nonspecific + Bilateral mesial temporal sclerosis	1 (1.4)

MRI diagnostic values in detecting hypomyelination & dys/demyelination pattern:

MRI had an excellent sensitivity, specificity and accuracy (92.3% 94.9% & 94.4% respectively) in correctly detecting hypomyelination pattern (Table 3).

Table 3: Diagnostic and predictive values of MRI hypomyelination pattern in diagnosing hypomyelinating disorders.

Hypomyelination pattern (Based on MRI)	Hypomyelination Group Based on final definitive diagnosis		Sensitivity	Specificity	PPV	NPV	Accuracy
	Positive (n = 13)	Negative (n = 59)					
Positive (n=15)	12	3	92.3	94.9	80	98.3	94.4
Negative	1	56					

PPV: Positive predictive value, NPV: Negative predictive value

MRI had high sensitivity, specificity and accuracy (88.1% and 92.3% & 88.9 % respectively) in correctly detecting dys/demyelination pattern (Table 4)

Table 4: Diagnostic and predictive values of MRI dys/demyelination pattern in diagnosing dysmyelinating and demyelinating disorders.

MRI Dys/Demyelination pattern (Based on MRI)	Dys/Demyelination Based on final definitive diagnosis		Sensitivity	Specificity	PPV	NPV	Accuracy
	Positive (n = 59)	Negative (n = 13)					
Positive (n=53)	52	1	88.1	92.3	98.1	63.2	88.9
Negative	7	12					

PPV: Positive predictive value, NPV: Negative predictive value

Correlation between MRI pattern and final groups of disorders (Table 5, 6);

There was a statistically significant correlation

between the MRI patterns of white matter signals including hypomyelination pattern and dys/demyelination pattern (confluent and multifocal patterns) and the final six groups of disorders. (Table 5)

Of the 13 cases diagnosed with hypomyelinating disorders, 12 exhibited an MRI pattern consistent with hypomyelination. All cases of CMD (n=7), ADS (n=15), and secondary demyelination (n=18) demonstrated distinct de/dysmyelination patterns on MRI. In contrast, only 8 out of 12 cases with IEM (also classified as dysmyelinating disorders) displayed de/dysmyelination patterns; the remaining 3 cases were incorrectly categorized as hypomyelinating. Notably, all CMD cases showed a confluent pattern (n=7), while the majority of ADS cases (13 out of 15) exhibited a multifocal pattern. (Table 5)

521

Table 5: Correlation between MRI patterns including: hypomyelination pattern and dys/demyelination patterns (confluent and multifocal) with final groups of definite diagnosis.

Final Definitive Diagnosis	Total (n = 72)	MRI patterns				P-v
		Hypomyelination (n = 15)	Dys/demyelination		Others (n = 4)	
			Confluent (n = 20)	Multifocal (n = 33)		
Hypomyelination	13 (18.1)	12 (80)	0	1 (3)	0	
IEM	12 (16.7)	3 (20)	3 (15)	5 (15.2)	1 (25)	
CMD	7 (9.7)	0	7 (35)	0	0	
ADS	15 (20.8)	0	2 (10)	13 (39.4)	0	0.03
Secondary demyelination	18 (25)	0	8 (40)	7 (21.2)	3 (75)	
Non-specific	7 (9.7)	0	0	7 (21.2)	0	

* P-values are based on Fisher Exact test. Statistical significance at P <0.05

The multifocal pattern was identified as the predominant characteristic in demyelinating diseases, while the confluent pattern was most prevalent in dysmyelinating diseases (P=0.03). However, when further subdividing the confluent and multifocal patterns into specific subgroups, no statistically significant differences were observed between dysmyelinating and demyelinating disorders. (Table 6).

Table 6: The subgroups of MRI pattern of dys/demyelination were correlated with the final diagnosis of dysmyelinating and demyelinating disorders.



MRI pattern	Final diagnosis group disorder		P-value
	Dysmyelinating disorders (n=15)	Demyelinating disorders (n=30)	
Dys/demyelination patterns			
Multifocal	5 (33.3)	20 (66.7)	0.03 ^a
Confluent	10 (66.7)	10 (33.3)	
Patterns of confluent pattern			
Bilateral symmetrical	9 (90)	6 (60)	0.3 ^b
Bilateral asymmetrical	1 (10)	4 (40)	
Patterns of multifocal pattern			
Patchy	3 (60)	15 (75)	0.5 ^b
Foci	2 (40)	5 (25)	

^a P-values are based on Chi square test. Statistical significance at P <0.05

^b P-values are based on Fisher Exact test. Statistical significance at P <0.05

MRI associated findings correlation with the assigned MRI white matter patterns (Table 7):

Table 7: Main MRI findings seen in the studied cases described according to pattern of MRI involvement of the white matter.

MRI findings	Total (n = 72)	MRI pattern				P-value
		Hypomyelination (n = 15)	Confluent pattern of dys/demyelination (n = 20)	Multifocal pattern of dys/demyelination (n = 33)	Others (n = 4)	
BG signal changes	15 (20.8)	0	4 (20)	11 (33.3)	0	0.043 ^a
Brain stem signal changes	8 (11.1)	0	3 (15)	5 (15.2)	0	0.56 ^b
Cerebellar WM hyperintensities	10 (13.9)	0	5 (25)	5 (15.2)	0	0.18 ^a
Cerebellar atrophy	4 (5.6)	0	2 (10)	1 (3)	1 (25)	
Cortical malformation	3 (4.2)	0	2 (10)	0	1 (25)	0.043 ^b
Diffusion restriction	11 (15.2)	0	5 (25)	5 (15.2)	1 (25)	0.21 ^a

^a P-values are based on Fisher Exact test. Statistical significance at P <0.05

^b P-values are based on Chi square test. Statistical significance at P <0.05

All BG changes (n=15) were observed exclusively in the dys/demyelinating pattern, with none detected in the hypomyelinating pattern. Notably, the majority of these changes (n=11/15) were concentrated in the multifocal pattern, which demonstrated a significant correlation with demyelinating diseases (p=0.043).

Cortical malformations primarily occurred in the confluent pattern of dys/demyelination (2 out of 3 cases), which is also correlated with dysmyelinating disorders (p=0.043).

Diffusion restriction, brain stem changes, cerebellar hyperintensities and cerebellar atrophy were not observed in any of the hypomyelinating disorders included in this study. Furthermore, no statistically significant differences were found in the prevalence of these MRI findings between the confluent and multifocal patterns of dys/demyelination.

Prevalence of correct diagnosis:

The prevalence of accurate pathological diagnoses achieved through multiparametric MRI analysis was found to be 88%, while the prevalence of correct etiological diagnoses was 85% (Chart 1). Furthermore, there was perfect inter-reader agreement among the three

observers, evidenced by a kappa coefficient of 0.91 (P < 0.001). This agreement was in the categorization of cases into patterns of hypomyelination and dys/demyelination, based on the white matter signal abnormalities detected on MRI.

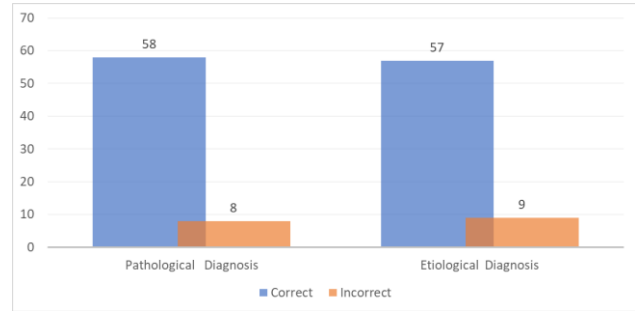


Chart 1: Prevalence of correct pathological and diagnosis etiological diagnosis (n=66)

Discussion

White matter diseases include wide spectrum of disorders prevalent in pediatric age group. A recent survey indicated that approximately 52% of the clinicians were moderately confident about providing a diagnosis and only 16 % were highly confident (7).

In our study we classified the patients based on the severity of the abnormal white signal intensity in MRI into two main categories: hypomyelination and dys/demyelination patterns. The Dys/demyelination pattern was further divided into confluent and multifocal patterns. Additionally, four cases exhibit other patterns of white matter involvement (cystic encephalomalacia, unilateral cerebral edema and reverse tigroid pattern) these were categorized separately as other group.

The Primary diagnosis of the cases studied was established using clinical data and MRI changes then compared to final diagnosis confirmed through targeted laboratory investigations, genetic analysis or follow up assessments. This comparison allows us to evaluate the sensitivity, specificity and accuracy of MRI in detecting each pattern.

Final diagnoses were classified into six main groups: hypomyelination, IEM, CMD, ADS, secondary demyelination and non-specific disorders. Variable MRI approaches were previously described in order to facilitate reaching correct diagnosis, primarily focusing on diagnosis of leukodystrophies and inborn errors of metabolism. One notable approach was presented that by Davies et al., 2023 (7), who employed a step wise evaluation method. They categorized cases



into those with predominantly white matter affection and those with substantial grey matter involvement. The predominant white matter cases were further classified into: hypomyelination and dysmyelination, with subgroups of the dysmyelination cases based on distribution patterns: subcortical, periventricular, diffuse, frontal and parieto-occipital distributions.

Our approach aligns with that by Davies et al. (2023) as we assessed all cases based on white matter signal characteristics into hypomyelination and dys/demyelination categories and in excluding neoplasms as well. However, unlike their approach we did not exclude demyelinating disorders or infections due to their relevance as diagnostic challenges for radiologists. Furthermore, unlike Davies et al. we divided the dys/demyelination group into: confluent pattern and multifocal pattern. The Confluent pattern was then subdivided into symmetrical and asymmetrical distribution, with the symmetrical distribution included: diffuse, periventricular, subcortical, and lobar predominance patterns, while the asymmetrical distribution was classified into periventricular and subcortical patterns.

The algorithm proposed by Sweatt et al. (2016) (9) was far similar to our approach with some minor differences. They classified MRI findings into: hypomyelination and non-hypomyelination (demyelination, dysmyelination). Similar to our approach, they divided the de/dysmyelination group into confluent (unifocal) or multifocal types, however their further division of the confluent type was different from ours. Their algorithm directly classified the confluent pattern into: diffuse, periventricular, subcortical, large asymmetrical, cerebellar & middle cerebellar, brainstem involvement, lobar predominance and classified multifocal type into: progressive, static or prominent perivascular spaces (9).

To our knowledge, no other studies have evaluated the diagnostic values and validity of various MRI patterns for diagnosing pediatric white matter diseases in a design similar to ours. However, Datar & Rupa (2018) assessed the validity and diagnostic utility of the MRI algorithm for white matter signal abnormalities suggested by Sweatt et al. (2016) (8).

The algorithm investigated by Datar and Rupa (8) demonstrated a sensitivity, specificity, and positive predictive value of 100%, 30%, and

74.1%, respectively. In contrast, our study reported the accuracy, sensitivity, and specificity for each MRI pattern of the two primary classifications as follows: for the hypomyelination pattern, the values were 94.4%, 92.3%, and 94.9%, while for the dys/demyelination pattern, they were 88.9%, 88.1%, and 92.3%. The observed differences may be attributed to several factors, including variations in sample size—Datar and Rupa analyzed data from 31 patients compared to our cohort of 72 patients—as well as differences in study populations; their research encompassed both pediatric and adult subjects (ages ranging from 5 to 948 months), whereas our study focused on a younger demographic (from 5 days to 192 months). Additionally, discrepancies may arise from the use of different algorithms in the respective studies.

In our study, all cases exhibiting MRI patterns indicative of dysmyelination or demyelination were diagnosed with corresponding dysmyelinating or demyelinating disorders, with the exception of one case. This particular case, which also presented an MRI pattern suggestive of dys/demyelination, was ultimately diagnosed as a hypomyelinating disorder—a rare and severe phenotype associated with a POLR3A variant involving striatal involvement. Seven cases with final diagnosis of dysmyelinating or demyelinating disorders, didn't show MRI pattern of dys/demyelination. Three cases displayed hypomyelination patterns, while the remaining four exhibited distinct patterns: two cases showed cystic encephalomalacia, one case demonstrated unilateral cerebral edema, and one case revealed a tigroid pattern.

Hypomyelination patterns were incorrectly identified in three cases (false positives), initially diagnosed as PMD but later confirmed as dysmyelinating disorders due to inborn errors of metabolism (IEM). These included glutaric aciduria type 1, metachromatic leukodystrophy, and isovaleric acidemia. Two of the cases involved patients aged 4 and 7 months, both exhibiting mild hyperintense signals on T2WI. Notably, follow-up imaging at one year showed no significant changes in the signal intensity of the white matter on T2WI. The third case involved a 17-month-old infant finally diagnosed with isovaleric acidemia through tandem mass spectrometry (TMS) and urinary organic acid analysis. This condition is a rare form of organic acidemia, with limited literature detailing its characteristic imaging findings. Previous reports have noted TWI hypointense and



T2WI hyperintense signals in the globus pallidi (10); however, these features were not observed in our case

One case ultimately diagnosed as a hypomyelinating disorder was initially classified within the dys/demyelination pattern. The primary MRI finding in this patient was a T2W hyperintense signal in the caudate and putamen, accompanied by significant atrophy. The white matter demonstrated only a few punctate hyperintensities. This case was misdiagnosed by consensus as Leigh syndrome (an IEM) based on MRI findings, Genetic testing subsequently identified a mutation in the POLR3A gene. A review of the literature indicated that this case did not present clinically or radiologically in a manner consistent with typical POLR3 mutations associated with 4H syndrome. However, a recent study has described a rare and severe phenotype of POLR3A variants involving striatal involvement (11). Consequently, this case was finally diagnosed as this rare severe phenotype.

The confluent pattern of white matter abnormalities was predominantly observed in dysmyelinating disorders, accounting for two-thirds of cases, with 90% exhibiting symmetrical distribution. Conversely, the multifocal pattern was primarily associated with demyelinating disorders, also comprising two-thirds of cases. These findings align with Schiffmann & Van Der Knaap. (2009), who noted that leukodystrophies typically present with bilateral, confluent, and symmetrical white matter changes, while ADs often display multifocal and asymmetrical patterns

The subdivisions of confluent patterns into symmetrical and asymmetrical distributions, as well as the multifocal patterns into patches and foci, did not reveal significant statistical differences between dysmyelinating and demyelinating disorders. This lack of significance may be attributed to the limited sample size within each category. Therefore, further investigation with larger cohorts is warranted to elucidate these distribution patterns more effectively.

Seven cases (9.7%) in our study exhibited only white matter foci (lesions < 5 mm), which did not fit into any established classifications from our algorithm and were classified as non-specific white matter signal changes on MRI; notably, one case presented with bilateral hippocampal mesial sclerosis. No definitive diagnosis for these white

matter abnormalities was established through multiparametric MRI. The predominant symptoms among these patients included seizures (57.1%), headaches (42.9%), and developmental delays (28.6%). In a related study by Wenger et al. (2023), 18% of children with white matter signal abnormalities were categorized as "nonspecific," with nearly half (48%) displaying multifocal lesions (13).

In our study a comprehensive assessment of BG, brainstem, posterior fossa structures and cerebral cortex using conventional MRI sequences (T1WI, T2WI and FLAIR) in addition to evaluating Diffusion restriction was done to detect any other associated abnormalities. We found a statistically significant difference in the prevalence of these changes between the hypomyelination and dys/demyelinating groups. Notably, none of the cases classified as hypomyelination by MRI showed any of these additional abnormalities. Interestingly, we had one case that was ultimately diagnosed as a severe phenotype of POLR3A variants with striatal involvement. This patient exhibited basal ganglia and brainstem changes along with brainstem diffusion restriction, yet was initially categorized as dys/demyelination based on the aforementioned MRI criteria. This case highlights the importance of considering atypical imaging findings, especially in rare disorders.

Although we did not find statistically significant differences among various MRI patterns, except for BG changes, the assessment of associated abnormalities was crucial for refining the differential diagnosis of white matter disorders and achieving accurate diagnoses. We did not identify any studies that specifically investigate these MRI changes to differentiate between the hypomyelination and dys/demyelination groups.

DWI and ADC assessments were conducted on all subjects, revealing diffusion restriction in only 11 cases (15.2%), all of which were classified within the dys/demyelinating group. Among these, one case was finally diagnosed with hypomyelination, specifically severe phenotype of POLR3A variants with striatal involvement. Additionally four cases were attributed to IEM, two cases of maple syrup urine disease, one case of Leigh syndrome, and one case of homocystinuria. Furthermore, six cases were finally diagnosed as viral encephalitis, ANEC, and postictal changes. The utility of diffusion imaging lies in its ability to differentiate various underlying pathologies; diffusion restriction is frequently observed in acute conditions such as



ischemic events, metabolic crises, acute demyelination, and infections (14).

Comparing primary diagnosis assigned to each case of our cases with its final confirmed diagnosis, excluding non-specific cases, revealed that the prevalence of reaching correct pathological diagnosis by integrated approach combining clinical data with MRI was 88%, additionally the accuracy for determining correct etiological diagnosis was 85%, and this discrepancy was because MRI was able to detect ischemic stroke, however, it failed to elucidate the underlying etiological causes of homocystinuria in two specific cases.

To date, no prior studies have assessed the inter-rater agreement in the classification of abnormal white matter signals into hypomyelination and dys/demyelination. However, Datar and Rupar (2018) reported a good level of agreement among their observers, with a Kappa statistic of 0.733, when evaluating their algorithmic approach to distinguishing between these types of white matter abnormalities.

Limitations

This study introduces a novel algorithm for diagnosing white matter diseases in children based on MRI findings; however, several limitations must be acknowledged.

Sample Size

A primary limitation is the small sample size of 72 cases, which may restrict the generalizability of the results and affect the statistical validity of some diagnostic criteria, as certain parameters did not yield statistically significant outcomes.

2-Validation

Despite its potential utility, the proposed algorithm requires further validation through larger-scale studies to enhance its robustness and applicability across diverse clinical settings.

3-Future Research Directions

We recommend future research to expand upon this work, ideally through collaborative efforts leading to a comprehensive meta-analysis. Integrating our findings with those from other studies could help establish a more definitive diagnostic algorithm for pediatric white matter diseases, ultimately improving diagnostic accuracy and patient outcome.

Conclusion

A thorough evaluation of conventional MRI

sequences, combined with advanced techniques like diffusion-weighted imaging, enhances diagnostic accuracy for pediatric white matter diseases. Further research with larger cohorts is recommended to refine these diagnostic approaches and improve patient outcomes.

Figure Legends

Figure 1. Flow chart for the pattern of distribution of white matter affection.

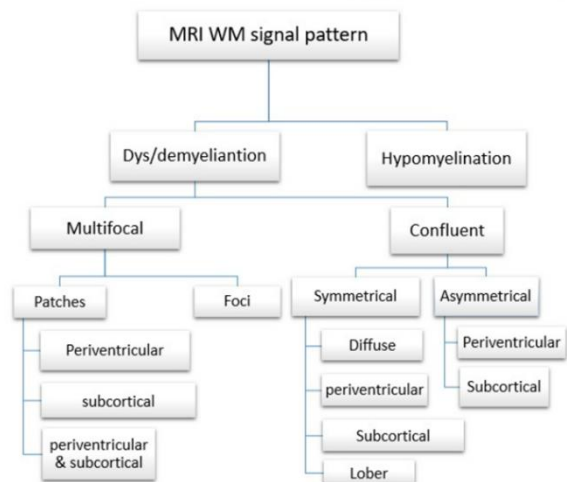


Figure 2. A 10-year-old female child, complaining of choreic movements with previous history of repetitive hospitalization due to chest infections. Axial FLAIR image (A) shows small hyperintense white matter foci in subcortical and deep white matter (white arrow head) in keeping with dys/demyelination pattern white matter foci. Axial T2WI image (B) shows bilateral atrophic, hyperintense putamen & caudate nuclei (black arrow heads). Axial T2WI (C) and DWI (D) showing signal hyperintensity at bilateral oculomotor nuclei (black arrow), with evidence of restricted diffusion (white arrow). Based on clinical presentation and imaging findings in basal ganglia and brain stem, the patient primarily diagnosed with Leigh Syndrome, however the final confirmed diagnosis was Severe phenotype of POLR3A variant with strial involvement, Hypomyelination.

Case 1

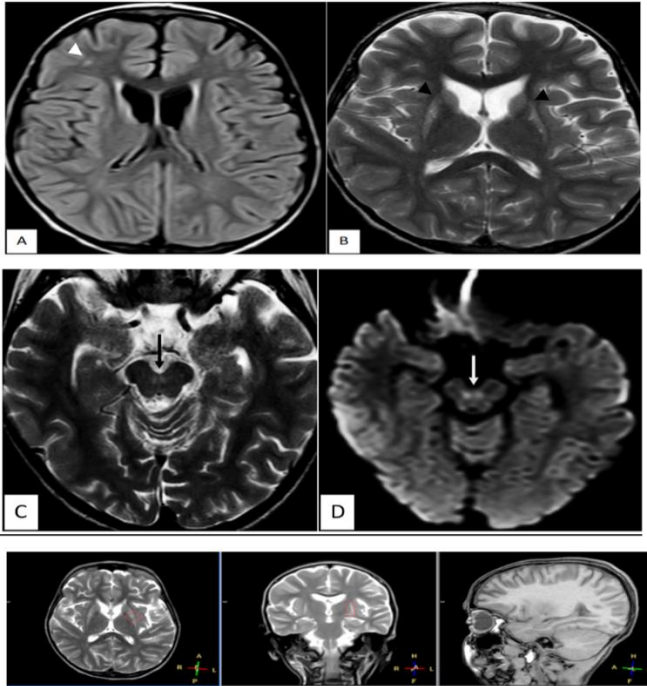


Figure 3. A 2-year-old male child complaining of disturbed level of consciousness after suffering fever for the last few days, fundus examination revealed bilateral optic atrophy. Axial T2WI at the level of basal ganglia (A) and centrum semiovale (B) shows bilateral confluent symmetrical diffuse involvement of the supratentorial white matter appreciated by all observers as being marked consistent with Dys/demyelination pattern in confluent, symmetrical & diffuse category. Axial T2WI (C) shows cerebellar dysplasia with cerebellar cysts (black arrow head). Midsagittal T1WI (D) showing pontine hypoplasia (white arrow head), vermian hypoplasia (white arrow) and small central cleft at corpus callosum (black arrow). The Primary and final diagnoses were concordant at this case as Muscle eye brain disease (MEB).

Case 2



Figure 4. A 4-year-old female infant, complaining of disturbed level of consciousness with history of febrile illness few days before. Axial T2WI (A) at level of basal ganglia and thalami, shows patchy hyperintense lesions in bilateral medial thalami, left lentiform nucleus and bilateral external capsules. Axial FLAIR image (B) shows patchy hyperintensities scattered at periventricular and subcortical white matter, consistent with Dys/demyelination pattern as described the three observers in multifocal, patchy, periventricular& subcortical manner. Axial T2WI images show hyperintense lesions at bilateral cerebellar peduncles (C) and cerebellar folia (D). Primary and final diagnoses, concordantly, were ADEM.



Case 3

Case 4

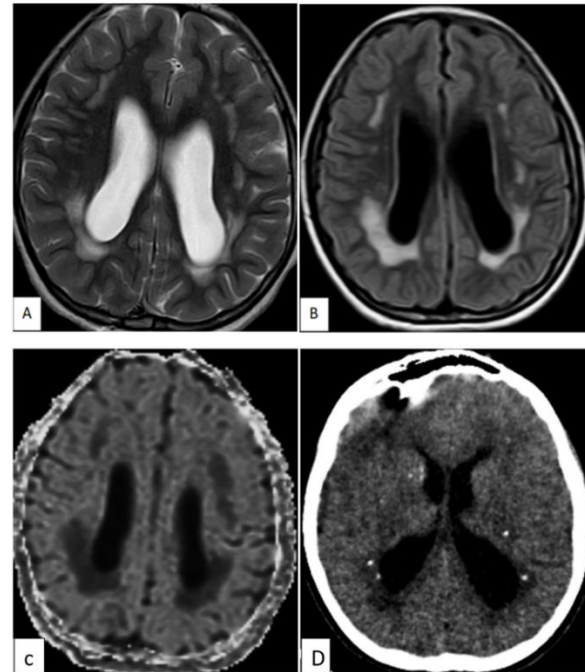
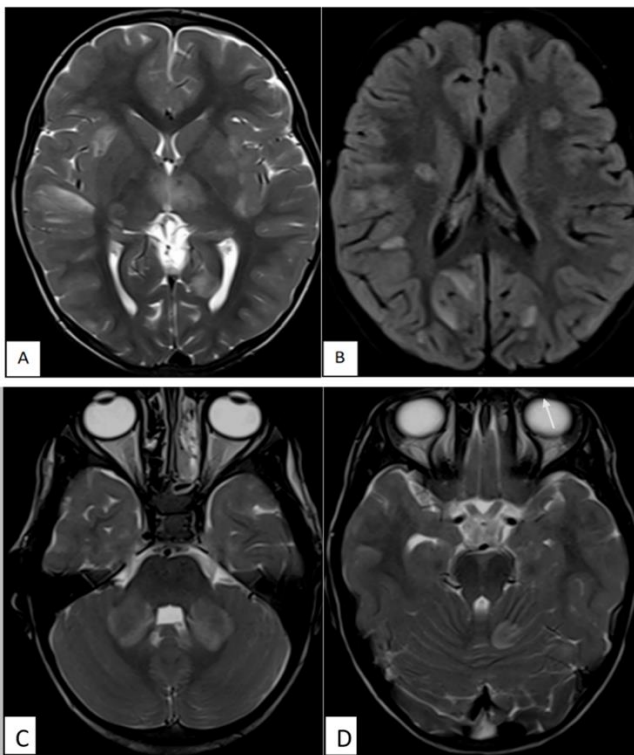


Figure 5. A 10-year-old male child, complaining of mental delay and convulsions. Axial T2WI (A) and axial FLAIR (B) at level of body of both lateral ventricles showing bilateral rather symmetrical confluent hyperintensities seen in periventricular white matter more evident posteriorly, interpreted by the observers as Dys/demyelination pattern, confluent, symmetrical, periventricular. Mild dilatation of both lateral ventricles is also noted. Axial DWI (C) shows facilitated diffusion of the white matter changes. Axial CT image (D) shows periventricular and basal ganglia calcifications. Primary and final diagnoses concordantly were congenital infection as (congenital CMV infection).

REFERENCES

1. Stadelmann, C. et al. (2019) 'Myelin in the central nervous system: Structure, function, and pathology', *Physiological Reviews*, 99(3), pp. 1381-1431.
2. Barkovich, A. J. (2005). Magnetic resonance techniques in the assessment of myelin and myelination. *Journal of Inherited Metabolic Disease*, 28(3),311-343.
3. Welker, K. M., & Patton, A. (2012). Assessment of normal myelination with magnetic resonance imaging. *Seminars in Neurology*, 32(1), 15-28.
4. Laule, C., Vavasour, I. M., Kolind, S. H., Li, D. K. B., Traboulsee, T. L., Moore, G. R. W., & MacKay, A. L. (2007). Magnetic Resonance Imaging of Myelin. *Neurotherapeutics*, 4(3), 460-484.
5. Ramji, S., Barkhof, F., & Mankad, K. (2019). Leukodystrophies and Inherited Metabolic Conditions. In *Clinical Neuroradiology*. https://doi.org/10.1007/978-3-319-68536-6_33.
6. Van der Knaap M, Valk J. (2005) Magnetic resonance of myelination and myelin disorders. 3rd ed. Berlin Heidelberg New York. p 1-19.
7. Davies, A., Tolliday, A., Craven, I., & Connolly, D. J. A. (2023). An approach to reporting paediatric leukoencephalopathy and leukodystrophies. *Clinical Radiology*, 78(6), 401-411.
8. Datar, R., Prasad, A. N., Tay, K. Y., Rupar, C. A., Ohorodnyk, P., Miller, M., & Prasad, C. (2018). Magnetic resonance imaging in the diagnosis of white matter signal abnormalities. *Neuroradiology Journal*, 31(4), 362-371.
9. Sweatt, S.K, Gower, B.A, Chieh, A.Y, Liu, Y, Li, L. (2016). 乳鼠心肌提取 HHS Public Access. *Physiology & Behavior*, 176(1), 139-148.
10. Sonia, F., Vernon, H. J., Huisman, T. A. G. M., & Bruno, P. (2018). Neuroimaging Findings of Organic. *Pediatric Imaging*, 38(3), 912-931.
11. Harting, I., Al-Saady, M., Krägeloh-Mann, I., Bley, A., Hempel, M., Bierhals, T., Karch, S., Moog, U., Bernard, G., Huntsman, R., van Spaendonk, R. M. L., Vreeburg, M., Rodríguez-Palmero, A., Pujol, A., van der Knaap, M. S., Pouwels, P. J. W., & Wolf, N. I. (2020). POLR3A variants with striatal involvement and extrapyramidal movement disorder. *Neurogenetics*, 21(2), 121-133.
12. Schiffmann, R., & Van Der Knaap, M. S. (2009). Invited Article: An MRI-based approach to the diagnosis of white matter disorders. *Neurology*, 72(8), 750-759.
13. Wenger, K. J., Koldijk, C. E., Hattingen, E., Porto, L., & Kurre, W. (2023). Characterization of MRI White Matter Signal Abnormalities in the Pediatric Population. *Children*, 10(2), 1-14.
14. Gaddamanugu, S., Shafaat, O., Sotoudeh, H., Sarrami, A. H., Rezaei, A., Saadatpour, Z., & Singhal, A. (2022). Clinical applications of diffusion-weighted sequence in brain imaging: beyond stroke. *Neuroradiology*, 64(1), 15-30.

